

**MULTIPARTICLE SIMULATIONS OF QUADROPOLAR ION DETECTION IN AN ION CYCLOTRON
RESONANCE CELL WITH FOUR NARROW APERTURE DETECTION ELECTRODES**

SUBMITTED TO JASMS

Running Title:

PIC SIMULATIONS OF A NADEL CELL

Joshua A. Driver^{*1}, Konstantin O. Nagornov^{*2}, Anton N. Kozhinov², Yury O. Tsybin², Andriy
Kharchenko^{1,3}, I. Jonathan Amster¹

¹University of Georgia, Department of Chemistry, Athens, GA 30602

²Spectroswiss Sàrl, EPFL Innovation Park, 1015 Lausanne, Switzerland

³NAS Institute of Cybernetics, Kyiv, Ukraine

* joint co-first authors, contributed equally to this manuscript

* Address for correspondence

Department of Chemistry, University of Georgia

Athens, Georgia 30602

Phone: (706) 542-2726

FAX: (706) 542-9454

Email: jamster@uga.edu

ABSTRACT

The current paradigm in FT-ICR cell design is to approximate the ideal 3-dimensional quadratic trapping potential as closely as possible to maintain ion cloud spatial coherence and achieve long transients, either with hyperbolically shaped electrodes, shimming electrodes, or by dynamic harmonization. In sharp contrast, the FT-ICR analyzer cell with four narrow aperture detection electrodes (NADEL) introduces significant anharmonic terms to the trapping potential. This analyzer cell is capable of quadrupolar detection, by which one can measure a signal that is close to the unperturbed cyclotron frequency. This is far less sensitive to trapping potential and space charge shifts than the reduced cyclotron frequency measured in conventional ICR cells. The quadrupolar mode of ion detection in NADEL cells has been examined previously by SIMION simulations of ion clouds with up to 500 ions per simulation. Here, the behavior of the NADEL analyzer cell is examined through particle-in-cell (PIC) simulations, which allows us to examine the behavior of large populations (tens of thousands) of ions with space charge considerations, and to calculate the induced charge on the NADEL detection electrodes, and thus the transient signal. PIC simulations confirm a unique spatial distribution of the ions, with a coherent motion that results in long transient signals. Dependence of the ion cloud and image current signal on cell design, ion energy, and magnetron radius are examined. Coalescence effects are compared to those found in a dynamically harmonized cell. The insensitivity of the measured cyclotron frequency to space-charge is demonstrated both with simulations and experimentally.

INTRODUCTION

FT- ICR mass spectrometry (FT-ICR MS) offers the highest mass accuracy and resolution of any mass spectrometer [1]. These features and others have made FT-ICR MS an important tool in many areas of study including proteomics and petroleomics [2-6]. Petroleum samples in particular require high mass accuracy, resolution, and dynamic range, due to the high peak density in their mass spectra. As ICR technology has improved, there has been increasing interest in designing new analyzer cells to obtain the highest resolution and the best mass accuracy.

Ions contained in a strong magnetic field will execute circular orbits, known as cyclotron motion, in a plane perpendicular to the field, with a frequency given by:

$$\omega_c = \frac{qB}{m} \quad (1)$$

where q is the charge on the ion, B is the magnetic field acting on the ion, and m is the ion's mass. To incorporate this principle in a mass spectrometer, the ions must be trapped along the magnetic field axis during the measurement of their cyclotron frequency, requiring the application of a static trapping field. In the quadratic trapping potential approximation, the trapping field perturbs the ion's motion, adding another periodic mode, called drift or magnetron motion, with a frequency given by [7]:

$$\omega_- = \frac{E_r}{rB} \quad (2)$$

where E_r is the radial component of the trapping electric field that repels ions away from the principal axis of the cell, and r is the radial displacement from that central axis. The frequency of the signal that is measured in a conventional FT-ICR MS is approximately equal to the

cyclotron frequency (ω_c) minus the magnetron frequency, (ω_-). This is known as the observed frequency or the reduced cyclotron frequency (ω_+). For cells with an ideal quadratic trapping potential, for which the ratio of electric field radial component to the radial displacement, $\frac{E_r}{r}$, is a constant over the volume of the cell, the spatial distribution of ions (generally, an ellipsoid of revolution) is maintained during the detection period. This provides a transient with a long period of duration, from the differential charge induced on an opposing set of detection electrodes. For simple analyzer cells (either cubic or cylindrical), additional, anharmonic terms are added to the gradient in the trapping field, meaning $\frac{E_r}{r}$ (and thus ω_-) is not constant throughout the analyzer cell. Consequently, the ion packet loses spatial coherence as ions oscillate along the trapping axis, due to the inhomogeneous nature of the radial electric field as a function of displacement along the z-coordinate [1]. This leads to the formation of a comet structure which accelerates damping of the transient signal, as the resulting symmetric distribution of ions does not produce an induced charge signal at ω_+ with dipolar detection circuits [8].

Analyzer cells with hyperbolically-shaped electrodes produce a purely quadratic trapping potential, and have been employed by physicists who make high precision mass measurements of atomic species [9]. However, the trapping volume of such a cell is small, and is not useful for analytical applications. To improve the resolution and mass accuracy of FT-ICR, efforts to improve analyzer cell design have focused on shimming the electric field to make it more closely match the ideal quadratic trapping potential, through static or dynamic harmonization [9-13]. This reduces variation in the magnetron frequency, thus improving ion

cloud coherence. A more coherent ion cloud can be measured for a longer period of time, increasing resolution.

In stark contrast to this design philosophy, a recent publication described an analyzer cell that deviates from the quadratic trapping potential. The Narrow Aperture Detection Electrodes (NADEL) cell [14], or NADEL, utilizes flat detection electrodes that extend in from the cylindrical excitation electrodes, toward the center of the analyzer cell [15]. These electrodes create a significant perturbation to the quadratic trapping potential, Figure 1, and the electric field gradient, $\frac{E_r}{r}$, varies considerably over the volume of the cell. Using both dipolar and quadrupolar ion detection, NADEL cells were able to demonstrate long transients, and high resolution, as well as a capability to detect the near unperturbed cyclotron frequency, $\omega_+ + \omega_- = \omega_c$ [15]. The latter feature makes the mass calibration less dependent on trapping voltage and space charge, and thus improves the frequency measurement precision and, consequently, the mass accuracy for experiments with strong variation of ion population.

This is not the first demonstration of the generation of the unperturbed cyclotron frequency, or even observing it as the primary signal. This concept was introduced by Schweikhard *et al.* in 1989 when he showed theoretically and experimentally that by using quadrupolar detection, one could generate two signals corresponding to $\omega_+ - \omega_-$ and $\omega_+ + \omega_-$, the latter being equal to the unperturbed cyclotron frequency [16]. It was later shown that by using two pairs of electrodes, the signal for the unperturbed cyclotron frequency could be increased, while the $\omega_+ - \omega_-$ signal was decreased [17]. If the magnetron radius is equal to the cyclotron radius, the $\omega_+ - \omega_-$ signal would decrease to zero [17]. However, these experiments used an analyzer cell with hyperbolic-shaped electrodes and were performed only on low mass ions.

Moreover, the intensity of second harmonic, $2\omega_+$, always remained higher than 20-30 % w.r.t. $\omega_+ + \omega_-$ signal, which is undesirable for real-life biological applications. Since that finding was published, this method has not been pursued in conventional ICR cells.

The NADEL cell design with 2 pairs of detection electrodes introduces significant anharmonic terms to the trapping field. Compared to other unshimmed analyzer cells, for example, the cubic cell, the cyclotron frequency can be observed without loss of signal or resolution. By conventional understanding and considering a tightly bunched ion distribution, one would expect the ion cloud to quickly lose coherence, leading to a swiftly decaying transient [8]. Instead, the signal was shown to be stable and produce the unperturbed cyclotron frequency, due to a unique cloud structure [15, 18]. SIMION simulations of up to 500 ions in NADEL cells suggested that phase-coherent spatial dispersion of ions in a non-linear, azimuthally-dependent electric trapping fields is responsible for the observation of frequency spectra at the unperturbed cyclotron frequency [19]. Each ion in such a field is characterized by its own cyclotron frequency with a center of the ion orbit drifting about the off-axis electric center of the trapping field. As a result, most if not all ions in a cell will contribute to the intensity of the cyclotron frequency peak but will introduce a destructive interference for the reduced cyclotron frequency peak [18, 19]. To gain further insights into the manner in which the NADEL cell is able to achieve this performance, one needs to consider the collective motion of the ions in more details, using multi-particle computer simulations with more features than offered by SIMION. Such simulations have shown to be a useful approach for examining the performance of FT-ICR analyzer cells, for example to accurately model the influence of subtle effects such as space-charge and ion-induced charge interactions [20-24]. Simulations provide

the ability to test the effects of parameters that are difficult to control experimentally such as the precise number, initial energy, and spatial distribution of ions in an analyzer cell [25]. The particle-in-cell (PIC) method, borrowed from the plasma physics community, offers a computationally tractable way to examine motion of realistic numbers of ions while maintaining an accurate account of space charge [26-28]. Additionally, the PIC method has been extended to include image charge forces on surfaces of arbitrary geometry, which is crucial to understanding the signal generated on the narrow detection electrodes [29].

EXPERIMENTAL

Multi-particle simulations were performed on z-cluster, a Linux cluster at the University of Georgia, on nodes equipped with Intel Xeon processors and NVIDIA K40m GPU cards. The PIC software is highly parallelized and uses the GPU cards to decrease calculation times. It also includes a parallelizable charge collocation based method for determining image charge, as described previously [29]. Simulations utilized a trapping potential defined by a SIMION model with the trapping plates set to 10 V. The simulations utilized a homogeneous magnetic field with a strength of 7 or 10 Tesla. The analyzer cell geometry is in accordance with a NADEL cell design with a diameter of 5.6 cm, a cubic cell of diameter 5.8 cm, or a dynamically harmonized cell composed of 8 hourglass/leaf electrode pairs with a diameter of 6 cm. The narrow detection electrodes stick into the NADEL 1.1 cm leading to an inscribed radius of 1.7 cm. For most simulations, a monoisotopic population of 1000 ions with $m/z = 524$ was generated with an ellipsoidal distribution (major axis = 2.5 mm; minor axis = 0.2 mm) with the major axis parallel to the magnetic field in the center of ICR cell and given an initial velocity (energy) in a line distribution of 0.2-0.4 mm/ μ s (0.11-0.43 eV) in the z-axis. These parameters were chosen

to generate maximum axial displacement in the NADEL cell, approximately 3.6 cm, just inside the annular trapping electrodes. Coalescence simulations instead used a 23^+ charge state of cytochrome c (22 most abundant masses in a theoretical distribution) with the same initial space and energy distribution and 50 V trapping potential. This high trapping voltage accelerates the process of coalescence, and reduced the computer simulation time to a tractable range.

A broadband chirp excitation from m/z 200 to m/z 10,000 over 5 ms with V_{p-p} of 25 V was used to excite ions to a higher cyclotron radius. The magnetron radius was then excited by applying DC potential of ± 5 V to opposing excite plates for a duration of 500 μ s after cyclotron excitation. A simulated time domain transient was collected for each experiment by summing the induced signal on opposing electrodes and subtracting the signal from orthogonal electrodes. This signal was sampled at 2 MHz for a duration of 0.5 s, followed by two zero-fills. No apodization was applied. A frequency domain spectrum was derived using FOM-AMOLF's AWE software [30]. Unless otherwise noted, experiments were performed with a quadrupolar detection scheme. The ion cloud and the resulting image charge distribution was visualized with in-house software developed at FOM-AMOLF [21]. A Fourier transform ion cyclotron resonance mass spectrometer (SolariX, Bruker Daltonics, Bremen, Germany) equipped with a 9.4 T superconducting magnet was employed to acquire all experimental data. The FT-ICR MS was equipped with the Paracell, also referred to as DHC cell, or the NADEL ICR cell (Spectroswiss, Lausanne, Switzerland) based on a design of an open-ended cylindrical ICR cell (Ultra cell, Thermo Scientific) as described elsewhere [31]. The NADEL ICR cell geometry represented a cylindrical surface with the four 90 degrees wide excitation electrodes and four narrow aperture detection electrodes [15]. NADEL

ICR cell had an aspect ratio of 2.5 (length of 140 mm and an inner diameter of 56 mm). The instrument was operated via standard in-built data acquisition station and instrument control software (Bruker Daltonics).

RESULTS AND DISCUSSION

NADEL cell with quadrupolar detection

As shown by Schweikhard [17], the signal for the unperturbed cyclotron frequency is maximized when the center of an ion's cyclotron orbit is offset from the center of the cell by a distance equal to the radius of its cyclotron orbit. This is consistent with experimental and computational (using SIMION) results with the NADEL cell [14, 15, 18], and these conditions were examined by PIC simulations. Figure 2a shows a calculated transient from a PIC simulation of quadrupolar detection in the NADEL ICR cell, with initial conditions selected that make the cyclotron radius approximately equal to the magnetron radius. The first 0.1 seconds of the transient shows the expected cyclotron frequency (~ 293055.7 Hz) superimposed on the magnetron frequency (~ 25 Hz). During this time, the ion cloud retains its initial structural qualities: tightly packed ellipsoid with all ions moving in coherent motion (Figure 2c). This result is consistent with the experiments performed by Schweikhard [16, 17], generating a peak at the unperturbed cyclotron frequency (ω_c) and two times the reduced cyclotron frequency ($2\omega_+$), the first due to combination frequencies ($\omega_+ + \omega_-$), the second due to measuring the coherent ion motion twice per cyclotron orbit.

After 0.1 seconds, however, the structure of the transient changes. Instead of the amplitude decay expected with dipolar detection, caused by comet formation, we see a stable

signal which no longer oscillates at the frequency of the magnetron motion. By tracking the motion of an individual ion as shown in Figure 2d, we can see that ions continue to undergo cyclotron motion, but with a distribution of their magnetron phase, leading to the formation of a rotating slab structure, in line with the previously obtained SIMION results [15]. The results of PIC simulations reported here confirm slab and star-like ion cloud structure formation as observed with SIMION simulations. Increased ion number in PIC simulations make slab formation and observation even more compelling. A video of the rotating motion of this novel ion cloud structure can be found in the supplementary material. During the first 0.2 seconds of the experiment, the ion cloud reorganizes to develop the slab distribution. Normally, the ions would spread along their cyclotron orbit, forming a comet, then a cylinder of charge once the head is reincorporated into the tail. However, because the magnetron radius is equal to the cyclotron radius, the dispersion of the ions along their cyclotron orbit does not form a cylinder. Instead, the collective motion of ions at different points in their cyclotron orbit creates the slab-like structure rotating on its major axis at half of the unperturbed cyclotron frequency. Figure 3 shows how the slab position corresponds to points in the sinusoidal image current. One can see from a comparison of the slab positions in inset A versus C, that as an ion rotates 180 degrees in its cyclotron orbit, the slab to which it belongs rotates 90 degrees. Thus, the slab rotates at half the cyclotron frequency, $(\omega_+ + \omega_-)/2 = \omega_c/2$. Since quadrupolar detection produces two maxima in the induced signal per slab rotation, all the ions in the slab generate a signal at the unperturbed cyclotron frequency. An additional explanation why the observed ion cloud structure rotates at half the cyclotron frequency has been published in relation to SIMION simulations of ion motion in NADEL cell [19].

This slab distribution forms when the cyclotron radius is equal to the magnetron radius, which is also the ideal ratio for generating the unperturbed cyclotron frequency through combination frequencies [17]. In the case of the NADEL cell with quadrupolar detection, the signal switches between these two modes of observing the unperturbed cyclotron frequency. Initially, ions are moving with coherent cyclotron motion at the reduced cyclotron frequency, generating a peak at $\omega_+ + \omega_-$ and $2\omega_+$. Within 0.2 seconds however, the slab ion distribution has formed, and generates an induced current signal at the unperturbed cyclotron frequency. Interestingly, since the slab-like structure is formed when ions are spread over their magnetron orbit, the ions do not have spatially-synchronized cyclotron orbits and, as a result, signal at $2\omega_+$ is slightly less than 5% of the base peak. Figure 2b shows the peak shapes and intensities in frequency space. Because of the non-linear trapping field, magnetron frequency appears as a broad distribution, which causes the reduced frequency, $\omega_+ = \omega_c - \omega_-$, to exhibit a similarly broad shape, as can be seen in the second harmonic peak, $2\omega_+$. In contrast, the signal at ω_c has no dependence on ω_- , and appears as a sharp, well-defined peak. Comparison of the signal intensities before and after the formation of the slab-like structure (supplementary material S1) shows that the intensity of the signal at ω_c is the same for the first 0.1 second and the last 0.1 second. The signal for $2\omega_+$, however, reduces 20-fold to only 1% of the base peak intensity. By processing the part of the transient acquired after this structure has formed, the unperturbed cyclotron frequency is the only signal of significant intensity in the spectrum, which confirms the reported earlier SIMION simulations and the experimental observations [15, 18].

Quadrupolar detection in DHC and Cubic cell analyzers

The detection of the unperturbed cyclotron frequency can be achieved with other cell geometries, but we expect those with ideal quadratic trapping potentials to maintain the initial ion cloud spatial distribution, and therefore produce other peaks, e.g. at $n\omega_+$ and $n\omega_+ \pm k\omega_-$, in addition to the signal at ω_c . This was examined with PIC simulations of both dynamically harmonized and cubic analyzer cells. Quadrupolar detection in a dynamically harmonized cell (DHC) resembles the experiments performed in a Penning trap by Schweikhard *et al.* [16, 17], as it has a nearly perfect 3D hyperbolic trapping field upon angular averaging [11]. Figures 2e and 2f show a simulated transient and the resulting frequency spectrum for quadrupolar detection in a DHC. To optimize quadrupolar detection for ω_c the cyclotron radius and magnetron radius are approximately equal. The frequency spectrum shows signals at ω_c , ω_+ , and $2\omega_+$. The transient features are consistent for the entire simulation (corresponding to a transient duration of 0.5 s) and visualization of the ion cloud (Figures 2g and 2h) shows that it does not dephase during this time. The first 0.1 s of the transient generates the same frequency spectrum as the 0.4 s-0.5 s section. This demonstrates that the signal at the unperturbed cyclotron frequency is due only to combination frequency detection, as no slab-like structure is generated. Since the ions maintain coherent cyclotron orbits, they continue to generate a signal at $2\omega_+$, increasing the complexity of the resultant spectrum. For a sample with many components, such as petroleum, this is undesirable. Although this analyzer cell does a nearly perfect job of replicating the ideal trapping field for dipolar detection, it is not ideal for use in detecting the unperturbed cyclotron frequency through quadrupolar detection since it continues to generate other frequencies.

Since the spatial dispersion of ions along their magnetron orbit is responsible for generating the unperturbed cyclotron frequency without also generating spurious frequencies, then it follows that any analyzer that deviates enough from an ideal trapping field should be able to replicate the results of the NADEL cell to some extent. A cubic analyzer cell is perhaps the simplest analyzer (although implementation of quadrupolar detection would be more complicated) and should work similarly to the NADEL cell in terms of detecting the unperturbed cyclotron frequency. Figures 2i and 2j show a simulated transient and the resultant frequency spectrum for quadrupolar detection in a cubic analyzer cell. Like the NADEL cell transient, the cubic cell transient is clearly divided into two parts; with the cyclotron signal superimposed on the magnetron signal early in the transient, followed by a stabilized signal that does not show magnetron oscillation. Visualization of the ion cloud (Figures 2k and 2l) shows that the cloud disperses along its magnetron orbit, leading to the rotating slab-structure. Analysis of the signal before and after the formation of the slab shows a drastic reduction in signal from $2\omega_+$ while ω_c remains the most intense peak.

Effect of space charge on ω_c and ω_+

A major benefit of detection at ω_c over ω_+ is the reduced dependence on space charge. To compare the effect of space charge on these different modes of detection, simulations were performed on a distribution of seven equally spaced peptide-like isotope packets ranging in m/z from 500 to 2000. By increasing the total number of ions present in the analyzer (quadrupolar detection in the NADEL cell or dipolar detection in the DHC), the frequency change was measured. Figure 4, left shows the change in frequency for the measured signal of the ion cloud at m/z 500 in the DHC and the NADEL cell. As the number of ions increase, the frequency

changes approximately 100 times more rapidly for ω_+ than ω_c . For ω_c the frequency changes in the opposing direction compared to ω_+ . Figure 4, right demonstrates the change in mass for 11 peaks of poly-phosphoric acid (H_3PO_4)_n in the mass range of 300 -1500 m/z experimentally measured with the DHC (Paracell) and the NADEL cell. As the number of ions increases, the mass (frequency) drifts approximately at least 5 times more rapidly for ω_+ than ω_c .

Effect of slab detection mode on coalescence

Ion cloud coalescence is an undesirable phenomenon caused by space charge interactions, which are accurately modeled by the PIC method. It occurs when ion clouds that are close in frequency phase-lock, appearing as a single peak in the mass spectrum [25]. This occurs at high ion density and results in a peak at a frequency corresponding to the average observed frequency of the coalesced ion clouds. The ions in the slab distribution have a lower charge density than in the ellipsoidal cloud typical of dipolar detection. The average radial distance between ions in the slab structure is 5.6 mm, compared to an average radial distance of 0.2 mm in the initial ion cloud before slab formation begins. Given this, one might expect slab mode detection to be less sensitive to ion cloud coalescence effects, but simulations show the onset of this behavior to occur with roughly the same number of ions in either mode of detection. To test this, we examined a simulated isotope distribution for cytochrome C (23+ charge state, $m/z \sim 512$). By increasing the number of ions in the simulation from 50,000 to 400,000 at a constant excite radius, the onset of coalescence can be observed. Figure 5 compares the mass spectra and ion positions at $t = 0.05$ s for increasing ion number in both the NADEL cell and a DHC. For this experiment, the goal was to compare quadrupolar detection in the NADEL cell with dipolar detection in the DHC. Both simulations are run at 50 V trapping,

with a cyclotron radius equal to 20 % of the cell radius (cylindrical electrodes have a 30 mm radius). The ions in the NADEL cell undergo magnetron excitation between cyclotron excite and detection, while the ions in the DHC are centered around the principal axis.

As can be seen in Figure 5, coalescence in the DHC and NADEL cell occurs at approximately the same rate. The DHC shows partial coalescence with 200,000 charges present and full coalescence with 400,000 charges. In contrast, the deterioration of signal in the NADEL cell is more consistent with ion cloud destruction. For example, the middle panel (200,000 charges) shows that the lower abundance ions (dark blue and red dots) have lost their slab structure, but the most abundant ions (light blue and blue green dots) still retain their slab structure. For the NADEL cell, there is very little ion cloud coalescence at 400,000 charges, even though the mass spectrum shows the merging of the isotope peaks into a single peak. It is important to note that the DHC can be potentially run at 2-4-fold higher cyclotron radius which should raise the charge threshold required for coalescence. A comparable simulation with excite radius equal to 40 % of the cell radius is shown in the supplementary material (S2). The maximum cyclotron radius will be limited in the NADEL cell due to the inward protruding detection electrodes. The inscribed radius of the detection electrodes could be increased to alleviate this, but might lead to a reduction in image charge intensity and other effects which would require further study to fully understand. Conversely, the DHC has a set aspect ratio of 2.6, but the NADEL cell used in these experiments had an aspect ratio of 1.5. Extending the NADEL cell would decrease the charge density without altering its other capabilities.

With the NADEL cell, space charge can upset the balance of magnetron radius and cyclotron radius even before detection begins. For dipolar detection, this would not noticeably

affect detection. However, for quadrupolar detection, this imbalance disturbs the formation of slab structures for many isotopes, leading to cloud destruction and, eventually, some coalescence. Effectively, at high charge density, the ion clouds in a NADEL cell are not participating in the same detection mode. The cyclotron frequency is still generated for high intensity and high mass ions, but the lower intensity and lower mass ion clouds do not form the necessary cloud structures for this mode of detection. Space charge can be a problem for slab formation and steps should be taken to reduce its effects during detection. This suggests that one of the anticipated advantages of quadrupolar detection in the NADEL cell, increasing the trapping voltage to hold more ions in the cell must be tempered with space charge limitations in mind. Quadrupolar detection in the NADEL cell reduces coalescence, but does not completely remove concerns of space charge.

Effect of ion z-axis energy on quadrupolar detection in the NADEL cell

Prior to formation of the slab structure, some reduced cyclotron coherence still exists, resulting in moderate signal intensity for the frequencies that depend on reduced cyclotron coherence (ω_+ and $2\omega_+$). If ions are quickly spread over the magnetron orbit, the signal at ω_c will be strong, but the magnetron frequency, ω_- , and therefore ω_+ and $2\omega_+$, will be distributed over many frequencies resulting in minimal intensity for these undesired peaks. Ideally detection should not start until the slab structure has formed. One method to make the slab structure form more quickly is to increase the ion z-axis energy and the spread of energies present, as suggested by the experimental and simulated data [15, 18]. Figure 6 demonstrates how increasing the ion energy spread results in quicker dephasing of the cloud as well as greater spread of ω_- , resulting in a lower intensity of $2\omega_+$. At even higher z-axial energy spreads, the ions dephase so quickly

that they do not present a coherent cloud during excitation of the magnetron radius. This leads to ions of the same -mass-to-charge having different ratios of magnetron radius to cyclotron radius, causing the ions to form a misaligned slab structure that eventually becomes isotropic. Adding a delay prior to detection that allows the slab to form and stabilize before signal is collected results in spectra with minimal contributions from ω_+ and $2\omega_+$. The length of this delay will depend on the range of energies present within each ion cloud as well as the trapping voltage [15, 18].

Effect of ratio of magnetron to cyclotron radius

Unless the electric trapping field closely approximates a 3D hyperbolic electric field, an ion cloud will adopt a more distributed structure even in the absence of neutral collisions. If the magnetron radius is zero, the ions will form a hollow cylinder of charge when the head of the comet is reincorporated into the tail [8]. This charge distribution is isotropic, and therefore undetectable. If, however, the magnetron radius is greater than zero but less than the cyclotron radius, loss of coherence instead forms an elliptical cylinder of charge, as shown in Figure 7. This cylinder will still be isotropic for the purposes of dipolar detection, but will generate a sinusoidal signal for quadrupolar detection at the ions' unperturbed cyclotron frequency. When magnetron radius equals cyclotron radius, the minor axis of the ellipsoid is zero, and the result is a rotating slab of charge. Further increases of the magnetron radius creates a mismatch between the alignments of the head and tail of the comet, leading to even more complex structures. Figure 7 shows how magnetron radius affects the shape of the ion cloud after dephasing.

Advantages of quadrupolar detection in the NADEL cell

Since the ions spread along their magnetron orbit to form the slab-like structure, a stable signal is produced as continued loss of coherence does not affect the shape of the cloud. Beyond stability, the signal generated from the slab-like structure has a few unique properties making it useful for accurate mass measurements. As with the signal generated through combination frequencies, the slab-like structure signal produces a peak at the unperturbed cyclotron frequency. This may allow mass calibration to be done without including a term for the magnetron frequency. Also, ω_c does not depend on the trapping voltage as ω_z does, meaning trapping voltages could be raised to increase the number of ions present in the analyzer cell, although space charge can still cause limitations. Additionally, since the magnetron frequency is not a single peak, but a very broad distribution, the signal does not produce a peak at $2\omega_z$, resulting in a spectrum that is not more complex than its dipolar detection counterpart.

The NADEL cell is particularly suited for quadrupolar detection for several reasons. The trapping field already deviates from the conventional trapping field enough to allow swift dephasing into the slab structure. The detection electrodes are also well designed for use here. Because the detection electrodes are narrow, quadrupolar detection can be performed without needing to use the same plates for excite and detect. With the NADEL setup, there can easily be four plates for detect, two for excitation of cyclotron motion, and two for excitation of magnetron motion. Additionally, a simple implementation of quadrupolar or quadrature ion excitation scheme can be done with NADEL ICR cell, possibly, further improving the performance of the observed phenomenon [32, 33]. Since the detection electrodes have lower

capacitance compared to the conventional 90 degrees electrodes and protrude into the analyzer cell, this setup can be utilized without loss in signal. Furthermore, the performance of the NADEL cell should be less sensitive to imperfections in its fabrication (machining tolerances, plate alignments, spacing), as ion behavior does not rely upon an adherence to the ideal quadratic trapping potential. In fact, a design with rectangular NADELs instead of the curved ones leads to further deviation from the quadratic trapping potential [14], which could lead to faster slab formation without higher trapping potential and improved excitation field in the plane along the magnetic field.

CONCLUSIONS

The NADEL cell design is a radical departure from high-performance ICR cell designs that seek to emulate the ideal 3D quadratic electric potential. Due to its unique properties, the NADEL cell has renewed interest in the concept of quadrupolar detection for use in accurate mass measurements. Through particle-in-cell ion trajectory calculations we have gained additional insight into how this method of detection works in the NADEL cell. The results obtained here are in line with and extend those from the previously reported SIMION simulations for the similar NADEL cell geometry but fewer number of charges (ions) [19]. We have confirmed here that quadrupolar detection can achieve stable and long-lived induced signals, despite the large non-quadratic terms in the trapping potential, and yet, it does not add complexity to the spectrum. This is achieved through the generation of a unique cloud structure that, once formed, does not undergo rapid decay. This results in long transients with highly accurate frequency (mass) measurements. Substantially reduced frequency shifts for increased ion numbers for NADEL cell compared to the DHC cell are suggested by PIC simulations and

confirmed with the experimental measurements. Although very high charge density can result in slab cloud destruction, careful experiment design will make this a useful tool in FT-ICR mass spectrometry.

ACKNOWLEDGEMENTS

The authors acknowledge the generous support of the National Science Foundation, grants CHE-1058913 and OISE-0730072, and the European Research Council (ERC Starting Grant 280271 to YOT)

REFERENCES

1. Amster, I. J., Fourier Transform Mass Spectrometry. *Journal of Mass Spectrometry* **31**, 1325-1337 (1996)
2. Terra, L. A.; Filgueiras, P. R.; Tose, L. V.; Romao, W.; de Souza, D. D.; de Castro, E. V. R.; de Oliveira, M. S. L.; Dias, J. C. M. and Poppi, R. J., Petroleomics by electrospray ionization FT-ICR mass spectrometry coupled to partial least squares with variable selection methods: prediction of the total acid number of crude oils. *Analyst* **139**, 4908-4916 (2014)
3. Bogdanov, B. and Smith, R. D., Proteomics by FTICR mass spectrometry: Top down and bottom up. *Mass Spectrometry Reviews* **24**, 168-200 (2005)
4. Kostyukevich, Y.; Kononikhin, A.; Popov, I.; Kharybin, O.; Perminova, I.; Konstantinov, A. and Nikolaev, E., Enumeration of Labile Hydrogens in Natural Organic Matter by Use of Hydrogen/Deuterium Exchange Fourier Transform Ion Cyclotron Resonance Mass Spectrometry. *Anal Chem* **85**, 11007-11013 (2013)
5. Smith, D. F.; Klein, G. C.; Yen, A. T.; Squicciarini, M. P.; Rodgers, R. P. and Marshall, A. G., Crude oil polar chemical composition derived from FT-ICR mass spectrometry accounts for asphaltene inhibitor specificity. *Energy Fuel* **22**, 3112-3117 (2008)
6. Marshall, A. G. and Rodgers, R. P., Petroleomics: Chemistry of the underworld. *P Natl Acad Sci USA* **105**, 18090-18095 (2008)
7. Tolmachev, A. V.; Robinson, E. W.; Wu, S.; Kang, H.; Lourette, N. M.; Pasa-Tolic, L. and Smith, R. D., Trapped-ion cell with improved DC potential harmonicity for FT-ICR MS. *J Am Soc Mass Spectrom* **19**, 586-597 (2008)
8. Nikolaev, E. N.; Heeren, R. M. A.; Popov, A. M.; Pozdnev, A. V. and Chingin, K. S., Realistic modeling of ion cloud motion in a Fourier transform ion cyclotron resonance cell by use of a particle-in-cell approach. *Rapid Commun Mass Sp* **21**, 3527-3546 (2007)
9. Gabrielse, G.; Haarsma, L. and Rolston, S. L., Open-Endcap Penning Traps for High-Precision Experiments. *International Journal of Mass Spectrometry and Ion Processes* **88**, 319-332 (1989)
10. Tolmachev, A. V.; Robinson, E. W.; Smith, R. D.; Leach, F. E.; Futrell, J. H. and Pasa-Tolic, L., A conceptual approach for FT-ICR cell harmonization utilizing external shim electrodes. *Int J Mass Spectrom* **325**, 45-50 (2012)
11. Nikolaev, E. N.; Boldin, I. A.; Jertz, R. and Baykut, G., Initial experimental characterization of a new ultra-high resolution FTICR cell with dynamic harmonization. *J Am Soc Mass Spectrom* **22**, 1125-1133 (2011)
12. Brustkern, A. M.; Rempel, D. L. and Gross, M. L., An electrically compensated trap designed to eighth order for FT-ICR mass Spectrometry. *J Am Soc Mass Spectr* **19**, 1281-1285 (2008)
13. Weisbrod, C. R.; Kaiser, N. K.; Skulason, G. E. and Bruce, J. E., Trapping ring electrode cell: A FTICR mass spectrometer cell for improved signal-to-noise and resolving power. *Anal Chem* **80**, 6545-6553 (2008)
14. Nagornov, K.; Kozhinov, A.; Tsybin, O. and Tsybin, Y., Ion Trap with Narrow Aperture Detection Electrodes for Fourier Transform Ion Cyclotron Resonance Mass Spectrometry. *J Am Soc Mass Spectr* **26**, 741-751 (2015)

15. Tsybin, Y. O.; Kozhinov, A. N. and Nagornov, K. O., Novel mass analyzers for rapid high-performance FT-ICR MS, *Proceedings of the 63rd American Society for Mass Spectrometry Conference on Mass Spectrometry and Allied Topics.*, 2015
16. Schweikhard, L.; Blundschling, M.; Jertz, R. and Kluge, H. J., A new detection scheme for Fourier transform - ion cyclotron resonance spectrometry in Penning traps. *Review of Scientific Instruments* **60**, 2631-2634 (1989)
17. Schweikhard, L.; Lindinger, M. and Kluge, H. J., Quadrupole-detection FT-ICR mass spectrometry. *International Journal of Mass Spectrometry and Ion Processes* **98**, 25-33 (1990)
18. Nagornov, K. O.; Kozhinov, A. N. and Tsybin, Y. O., Fourier Transform Ion Cyclotron Resonance Mass Spectrometry at the Cyclotron Frequency. *J Am Soc Mass Spectr* 1-13 (2017)
19. Nagornov, K. O.; Kozhinov, A. N. and Tsybin, Y. O., Cyclotron phase-coherent ion spatial dispersion in a non-quadratic trapping potential is responsible for FT-ICR MS at the cyclotron frequency. *J Am Soc Mass Spectr* in press
20. Nikolaev, E. N.; Kostyukevich, Y. I. and Vladimirov, G. N., Fourier transform ion cyclotron resonance (FT ICR) mass spectrometry: Theory and simulations. *Mass Spectrometry Reviews* n/a-n/a (2014)
21. Burakiewicz, W. and van Liere, R., Analyzing complex FTMS simulations: A case study in high-level visualization of ion motions. *Ieee Transactions on Visualization and Computer Graphics* **12**, 1037-1043 (2006)
22. Kharchenko, A.; Vladimirov, G.; Heeren, R. M. A. and Nikolaev, E. N., Performance of Orbitrap Mass Analyzer at Various Space Charge and Non-Ideal Field Conditions: Simulation Approach. *J Am Soc Mass Spectr* **23**, 977-987 (2012)
23. Leach, F. E.; Kharchenko, A.; Vladimirov, G.; Aizikov, K.; O'Connor, P. B.; Nikolaev, E.; Heeren, R. M. A. and Amster, I. J., Analysis of phase dependent frequency shifts in simulated FTMS transients using the filter diagonalization method. *Int J Mass Spectrom* **325**, 19-24 (2012)
24. Leach, F. E.; Kharchenko, A.; Heeren, R. M. A.; Nikolaev, E. and Amster, I. J., Comparison of Particle-In-Cell Simulations with Experimentally Observed Frequency Shifts Between Ions of the Same Mass-To-Charge in Fourier Transform Ion Cyclotron Resonance Mass Spectrometry. *J Am Soc Mass Spectr* **21**, 203-208 (2010)
25. Vladimirov, G.; Hendrickson, C. L.; Blakney, G. T.; Marshall, A. G.; Heeren, R. M. A. and Nikolaev, E. N., Fourier Transform Ion Cyclotron Resonance Mass Resolution and Dynamic Range Limits Calculated by Computer Modeling of Ion Cloud Motion. *J Am Soc Mass Spectr* **23**, 375-384 (2012)
26. Birdsall, C. K., Particle-in-cell charged-particle simulations, plus Monte Carlo collisions with neutral atoms, PIC-MCC. *Plasma Science, IEEE Transactions on* **19**, 65-85 (1991)
27. Mitchell, D. W., Realistic simulation of the ion cyclotron resonance mass spectrometer using a distributed three-dimensional particle-in-cell code. *J Am Soc Mass Spectr* **10**, 136-152 (1999)
28. Mitchell, D. W. and Smith, R. D., Two dimensional many particle simulation of trapped ions. *Int J Mass Spectrom* **165**, 271-297 (1997)

29. Driver, J. A.; Kharchenko, A.; Heeren, R. M. A. and Amster, I. J., Fast image-charge calculations for multi-particle simulations in FT-ICR analyzer cells of arbitrary geometry. *Int J Mass Spectrom* **377**, 432-439 (2015)
30. Mize, T. H.; Taban, I.; Duursma, M.; Seynen, M.; Konijnenburg, M.; Vijftigschild, A.; Doornik, C. V.; Rooij, G. V. and Heeren, R. M. A., A modular data and control system to improve sensitivity, selectivity, speed of analysis, ease of use, and transient duration in an external source FTICR-MS. *Int J Mass Spectrom* **235**, 243-253 (2004)
31. Tolmachev, A. V.; Robinson, E. W.; Wu, S.; Kang, H.; Lourette, N. M.; Paša-Tolić, L. and Smith, R. D., Trapped-ion cell with improved dc potential harmonicity for FT-ICR MS. *J. Am. Soc. Mass Spectrom.* **19**, 586-597 (2008)
32. Pitsenberger, C. C.; Easterling, M. L. and Amster, I. J., Efficient ion remeasurement using broadband quadrupolar excitation FTICR mass spectrometry. *Anal Chem* **68**, 3732-3739 (1996)
33. Guan, S. H.; Gorshkov, M. V. and Marshall, A. G., Circularly Polarized Quadrature Excitation for Fourier-Transform Ion-Cyclotron Resonance Mass-Spectrometry. *Chem Phys Lett* **198**, 143-148 (1992)

FIGURE CAPTIONS

Figure 1. Comparison of electric fields in SIMION models of a 3D quadratic trapping potential, NADEL cell and cubic cell. The 3D quadratic trapping potential causes no (a) angular or (b) axial variation in E_r/r , and there are no perturbations to in the (c) potential contour lines. In fact, all data points are the same because E_r/r is a constant for this cell. The NADEL cell, in contrast, has simple trapping electrodes and inward protruding detection electrodes that cause (d) axial and (e) angular variation in E_r/r respectively. The (f) potential contour lines at the center of the analyzer for the NADEL cell show the perturbations caused by the protruding detection electrodes. A cubic cell produces (g, h) variations in E_r/r and (i) perturbations to the contour lines that are very similar to those produced by the NADEL cell.

Figure 2. Comparison of quadrupolar detection in (a-d) NADEL cell, (e-h) DHC, and (i-l) cubic cell. (a,e,i) Simulated transients and (b,f,j) resulting frequency spectra. Visualization of the ion positions at (c,g,k) $t = 0.0$ s and (d,h,l) $t = 0.5$ s. The red circles describe cyclotron orbits for one or two ions in the simulation; blue circles describe the ions' magnetron orbit. For the NADEL simulation, colored dots show ion positions over the next cyclotron orbit starting at blue and going to red.

Figure 3. Simulated transient signal with corresponding ion positions showing detection of the slab-like clouds. The detection electrodes are shown as red (negative) and blue (positive) points and the transient at each time step is calculated by the image charges on the blue electrodes minus the image charge on the red electrodes. The red circle

describes a single ion's cyclotron orbit over this 4 μ s period. The slab rotates 180 degrees in the same amount of time it takes an ion to complete its cyclotron orbit, resulting in the slab rotating at half of the cyclotron frequency.

Figure 4. Comparison of the effect of space charge on detection at ω_c and ω_+ .

(Left) shows results of PIC simulations. (Right) the mass error dependence on the number of charges (total ion current) was experimentally measured using the 9.4 T SolariX FT-ICR MS with the Paracell or the DHC cell (blue circles) or the NADEL cell (red circles) for the 11 monoisotopic peaks of a poly-phosphoric acid (H_3PO_4)_n in the mass range of 300 -1500 m/z in a number of single scans. The number of charges (total ion current) was varied via changing the ion accumulation time in an external ion trap before ion transfer into the corresponding ICR cells. The same set of mass calibration coefficients was employed for the experiments with Paracell (DHC) and NADEL ICR cell.

Figure 5. Comparison of DHC and NADEL cell ion clouds and simulated mass spectra for cytochrome C 23⁺ charge state. (left) Mass spectra for DHC and NADEL cell with increasing numbers of charges present (50,000 top, 200,000 middle, and 400,000 bottom). (right) Ion positions 0.05 s after the start of detection. Colors correspond to individual m/z values as shown on the mass spectra. The DHC signal is observed at the reduced cyclotron frequency leading to higher m/z values if not calibrated.

Figure 6. Increasing ion energy spread for 1000 ions in the NADEL cell where $V_t = 50$ V. As the initial energy increases, the ions can move farther along the z-axis, increasing the disparity between E_r/r . This results in a wider array of magnetron frequencies, reducing the intensity of the peak at $2\omega^+$.

Figure 7. Ion cloud structure development as magnetron radius (R_m) approaches cyclotron radius (R_c). These ion clouds will produce no signal in dipolar detection after 0.15 s, but will still be detectable by quadrupolar detection, with $R_m = R_c$ producing the most intense signal. Furthermore, the signal from the first three cloud structures will not deteriorate due to the electric fields. For $R_m > R_c$, the head and tail of the ion cloud do not meet up within the timeframe shown here, and the ions will continue to spread around the analyzer cell.

Figure 1.

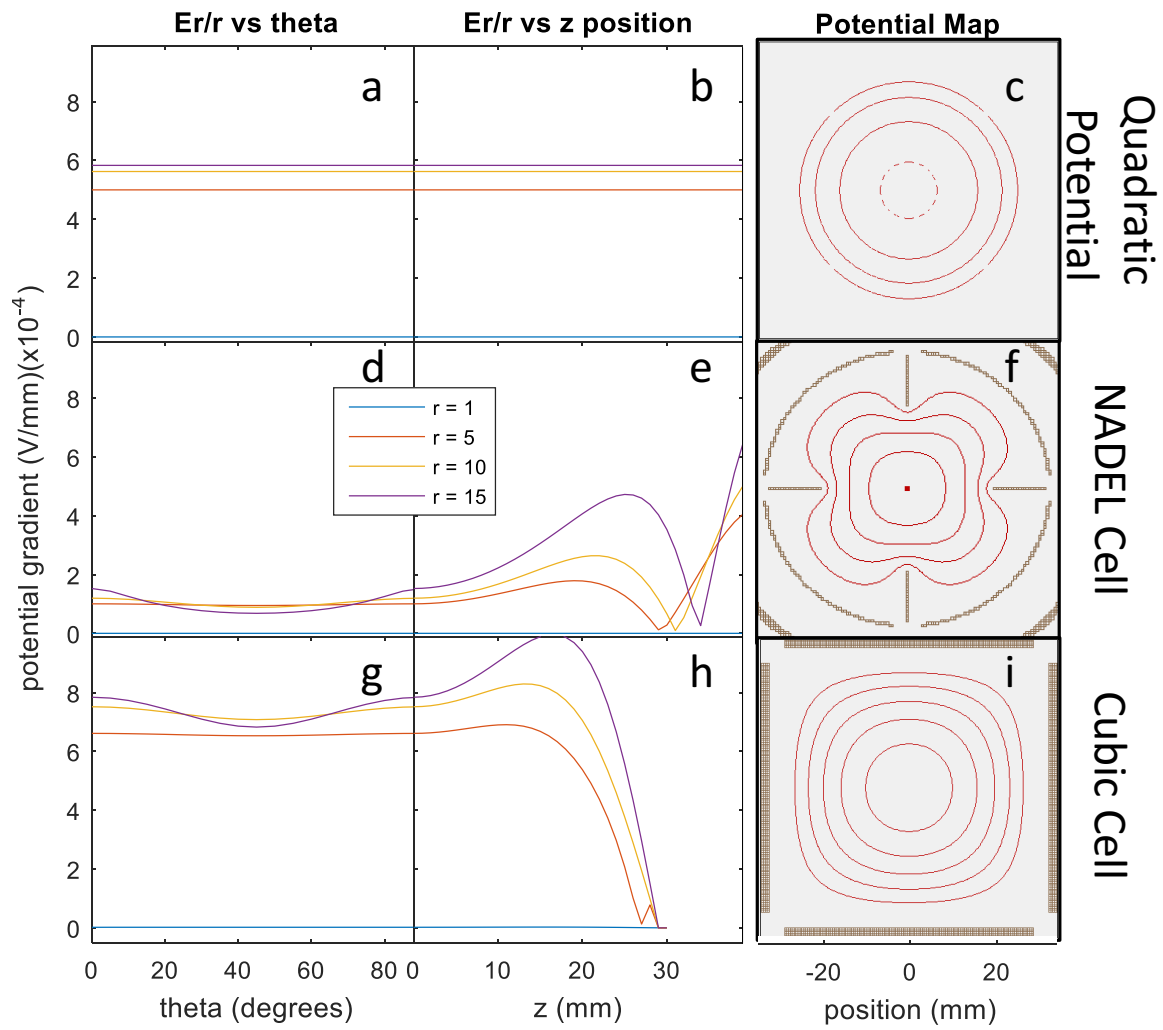


Figure 2.

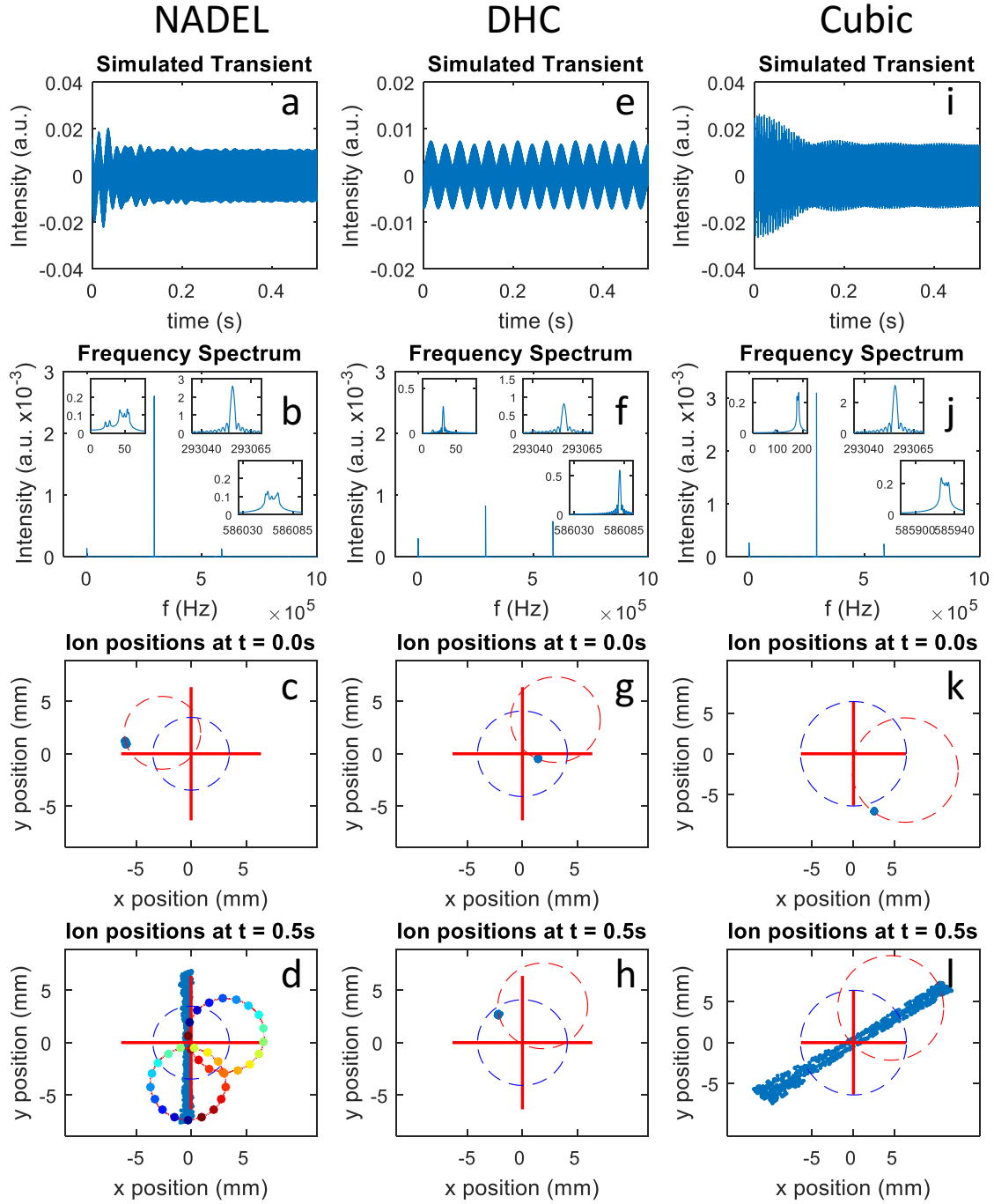


Figure 3.

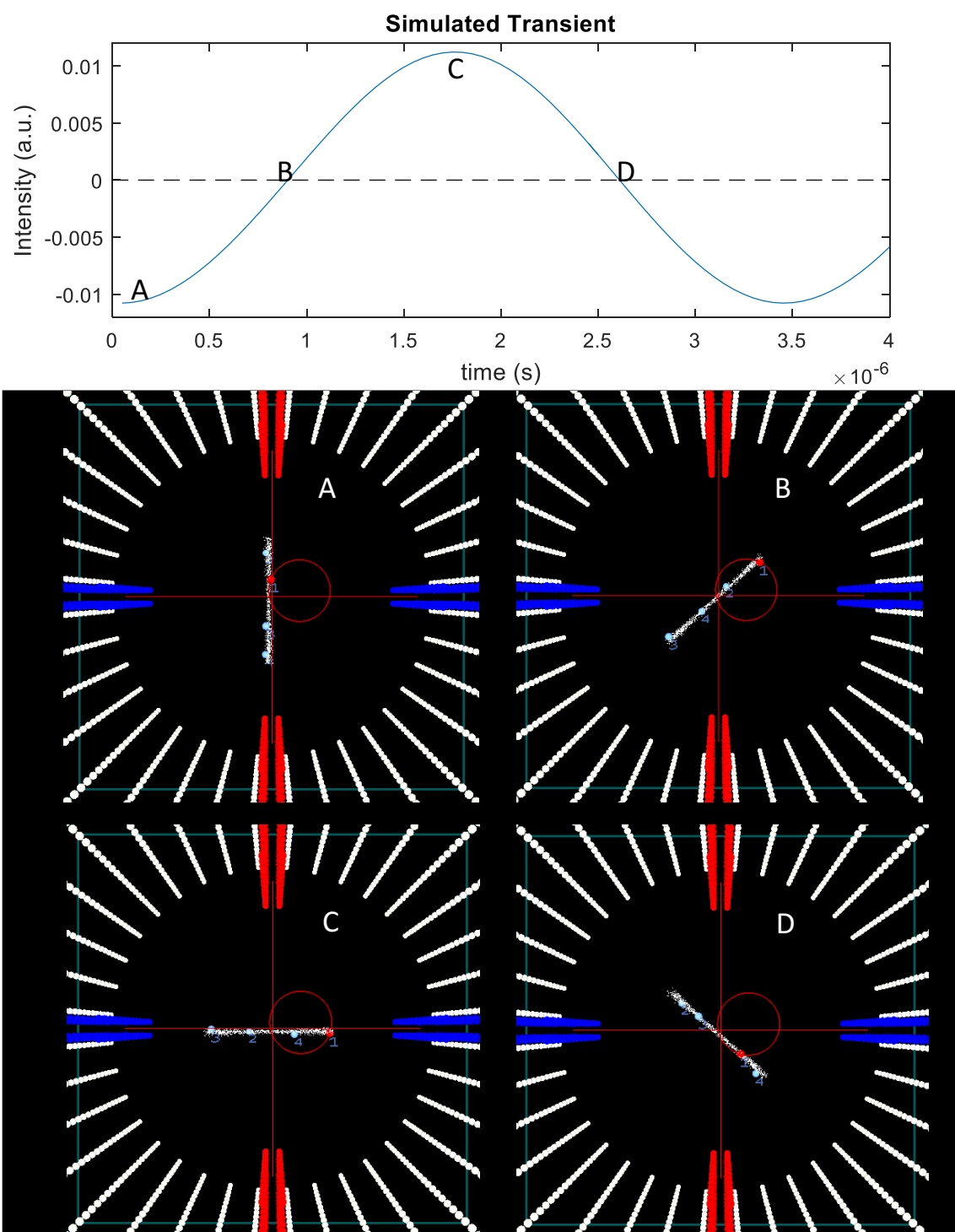


Figure 4.

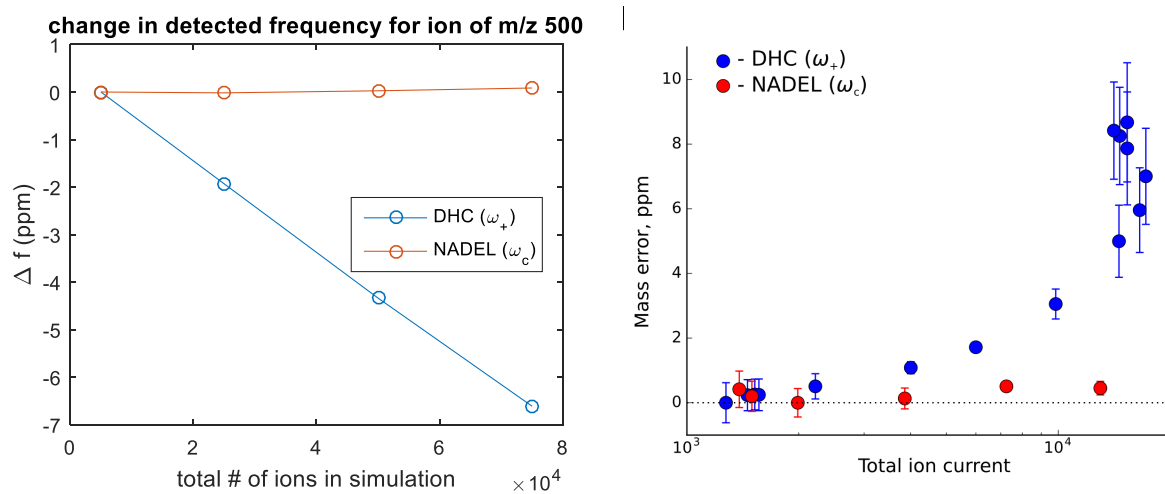


Figure 5.

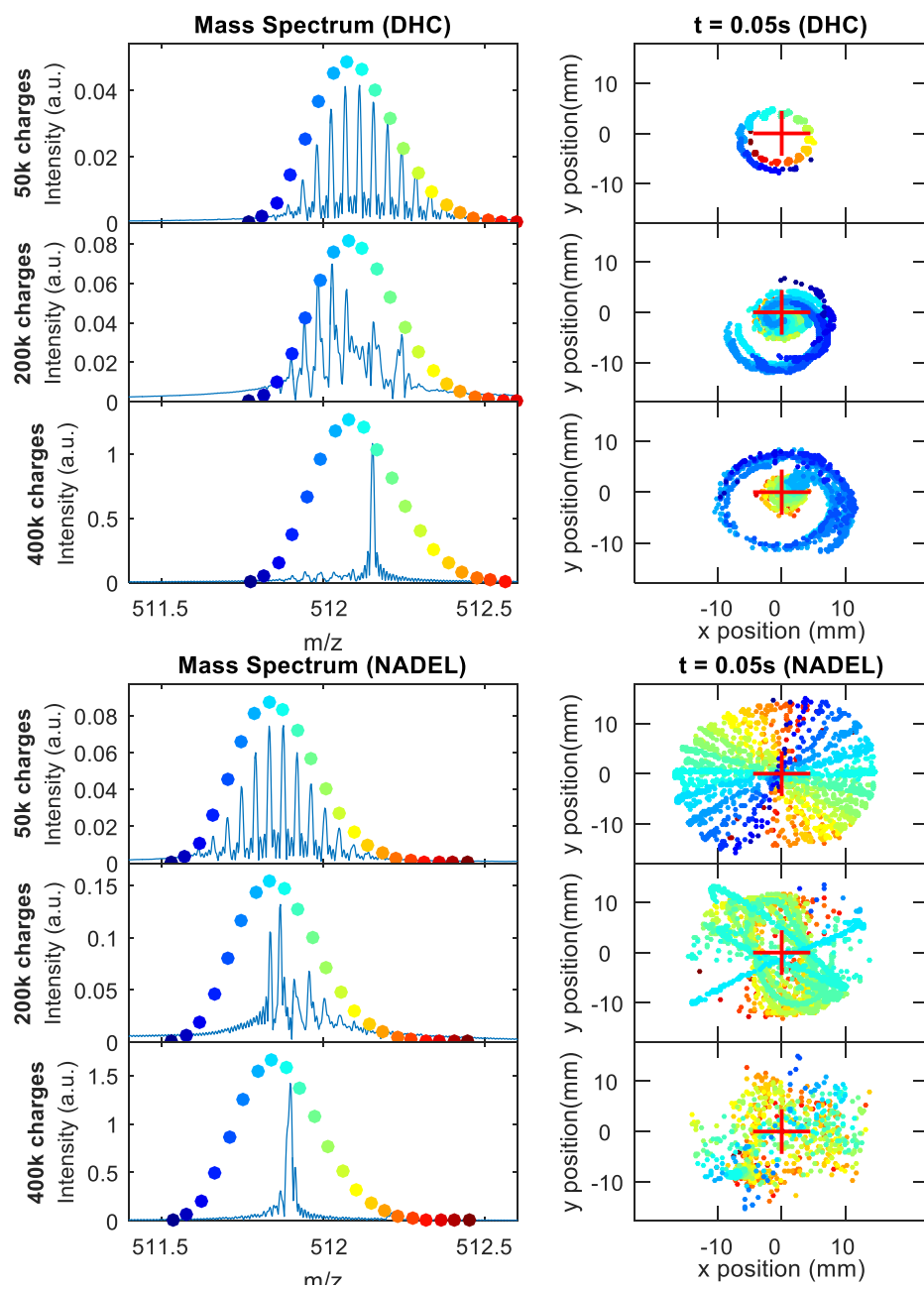


Figure 6.

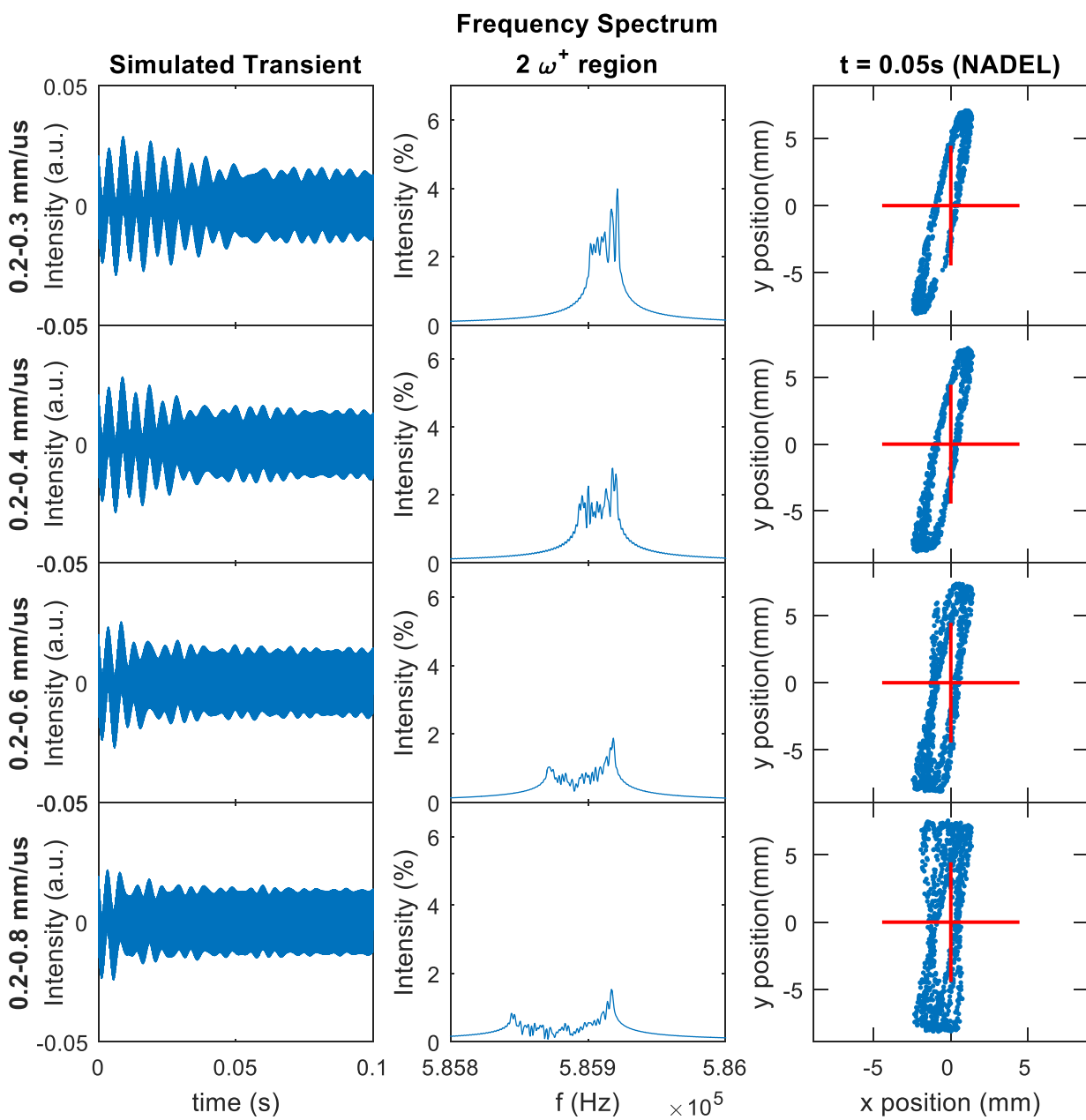


Figure 7.

